

CFD Simulation on Flow Field of a Large Flow Rate High Speed On/off Valve

Qiang GAO, Yuchuan ZHU*, Xiaoming CHEN, Bruno Niyomwungeri

(College of Mechanical and Electrical Engineering,

Nanjing University of Aeronautics and Astronautics, Nanjing 210016, China)

gaoqiang116@nuaa.edu.cn, meeyczhu@nuaa.edu.cn

Abstract—The large flow rate high speed on/off valves (LFHSV) have often been used to control flow or pressure in large power applications due to its fast switching. However, the applications of LFHSV are limited by vibration and noise. In this paper, CFD simulations of a two-stage LFHSV are conducted to analyze the flow field characteristics of the main poppet valve, including flow simulation under fixed opening and the transient flow simulation. Results showed that there are two vortexes formed in the flow channel which extract the energy from the main flow and intensify the fluid noise, and that the inlet pressure peak increases by 8.6% in the closing stage. The results will provide guidance for the optimal structural design of high speed on/off valves.

Keywords—High speed on/off valve, large flow rate, CFD, Dynamic mesh, Pressure peak

I. INTRODUCTION

Digital hydraulic systems are considered as a new branch of fluid power, which offer high potential for innovative technologies [1]. Compared with the conventional electro-hydraulic servo systems, the digital hydraulic systems have advantages of high efficiency and high reliability [2]. High speed on/off valve (HSV) which are considered to be the core component of the digital hydraulic system has been employed in several applications, such as aircraft brake system [3], antilock braking system [4] and so on, due to its low cost, high reliability and robustness[5][6].

However, vibration and noise are the serious problems which limit the application of the HSV. These issues are extremely complicated due to the coupling among the mechanical, oil and air. The recent developments in Computational fluid dynamics (CFD) make it possible to achieve a better understanding of flow dynamics. Guo et.al [7] developed a new 6DOF method to simulate the movement of a three-dimensional poppet valve which is determined by fluid force, gravity and other forces. Yang et.al [8] proposed a new optimal design of the valve cone angle and the coordinate angle. In the study, the fluid noise is reduced over 5 dB which is verified by CFD method. Gao et.al [9] studied the velocity distribution of a poppet valve using Galerkin finite element methods and digital particle image velocimetry (DPIV), and the results have a practical significance for structural optimization design.

In order to achieve a good understanding of the flow field of the HSV, in this paper, a two-stage large flow rate high speed on/off valve is used as a research object. Firstly, the structure and working principle are presented. Secondly, the flow simulation under fixed opening is carried out to analyze the causes of vortexes formation

which is related to the energy efficiency and fluid noise. Finally, the transient flow simulation is conducted based on dynamic mesh technique to analyze the pressure peak and fluid hammer. The simulation results can provide guidance for the optimal structural designs of large flow rate high speed on/off valves.

II. STRUCTURE AND MODEL

A. Structure and Working principle

Figure 1 shows the schematic diagram of the two-stage large flow rate high speed on/off valve (LFHSV). It consists of a pilot HSV, a main valve body, a main poppet valve (normally closed), a spring, an adjusting rod, and an end cap. The pilot valve is a 2-position and 3-way normally opened HSV. The method of chamfer equalizer-slot is used in the main poppet valve to prevent oil leakage from the control chamber to the outlet of the main valve. The annular gap between the main poppet valve and the main valve body is kept within 0.015mm. The spring is used to provide a certain pre-pressure to ensure that the main valve is reliably closed. The adjusting rod is used to limit the maximum displacement of the main valve. The advantage of the proposed LFHSV is that the maximum flow rate can be adjusted to meet the requirements of different applications.

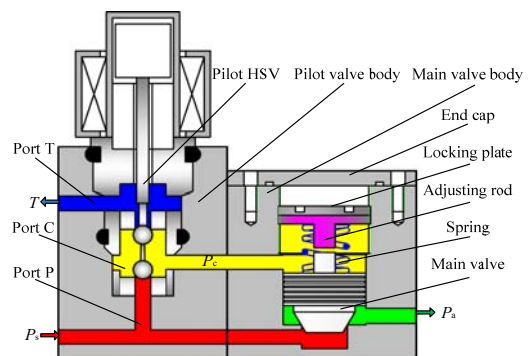


Figure 1. Schematic diagram of the LFHSV

Initially, when the coil is de-energized, the pilot ball valve is pushed upward by the high pressure from port P. In that case, port C is connected to port P and port T is blocked. The main poppet valve will be closed due to the area difference between the supply chamber and the control chamber. Conversely, when the coil is energized, the pilot ball valve pushed downward by the electromagnetic force. Like that, port C is connected to port T, port P is blocked and the main poppet valve opens due to the pressure difference between the supply chamber and the control chamber.

B. Mathematical Model

Based on Newton's laws of motion and kinetic equations in general, the force balance equation of the main valve can be described by

$$m_p \ddot{x}_m = A_{ms} p_s + A_{ma} p_a - A_c p_c + F_f - k_m(x_0 + x_m) - B_m \dot{x}_m \quad (1)$$

Where x_m and m_p denote the displacement of the main valve and the mass of the main valve, respectively. A_{ms} , A_c and A_{ma} denote the area of the inlet side of the main valve, the control chamber and the outlet side of the main valve, respectively. k_m denotes the stiffness of the spring. x_0 denotes the preload length of the spring. B_m and F_f denote the damping constant of the main valve and the steady flow force of the main valve, respectively. p_s , p_c and p_a denote the inlet pressure, the control pressure and outlet pressure, respectively.

The flow area of the main valve can be expressed as:

$$A_m = \pi x_m \sin \theta_m (D - x_m \sin \theta_m \cos \theta_m) \quad (2)$$

Then, the average flow rate of the main valve actuated by the PWM signal is as follows:

$$Q_m = c_d A_{max} \tau \sqrt{\frac{2}{\rho} (p_s - p_a)} \quad (3)$$

Where θ_m and D denote the half cone angle of the main valve and the diameter of the main valve inlet; τ denotes the duty cycle of the PWM signal; A_{max} and c_d denote the maximum flow area of the main valve and the flow coefficient, respectively.

The momentum equation of the inlet fluid control volume and the outlet fluid control volume (Figure 2 (a)) are as follows[10]:

$$\rho Q_m v_j \cos \alpha - \rho Q_m v_s \cos(\pi/2) = F_s - F_{fi} - F_j \quad (4)$$

$$\rho Q_m v_a \cos(\pi/2) - \rho Q_m v_j \cos \alpha = F_z + F_{fo} - F_{fo} \quad (5)$$

The momentum equation of the whole fluid control volume based on equation (4) and (5) is as follows:

$$0 - 0 = F_s + F_z - F_{fi} - F_{fo} \quad (6)$$

So the steady flow force can be written as:

$$\begin{aligned} F_f &= F_{fi} + F_{fo} - p_s A_0 - p_a A_a \\ &= F_s + F_z - p_s A_0 - p_a A_a = F_z - p_a A_a \end{aligned} \quad (7)$$

Where v_s , v_a , and v_j denote the inlet velocity, the outlet velocity, and the jet cross section velocity. F_{fi} , F_{fo} and F_j denote the steady flow force in the inlet chamber, in the outlet chamber and at the jet cross section, respectively. F_z denotes the reaction force of the seat on the liquid. α denotes the average jet angle of liquid. To calculate the F_z , the rotation surface is shown in Figure 2 (b).

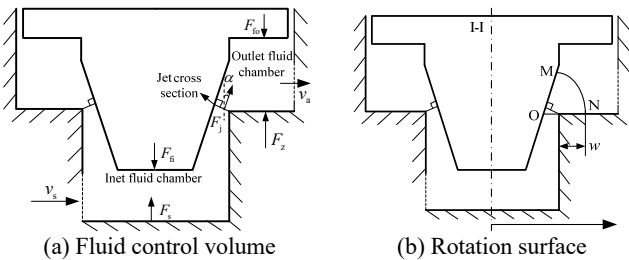


Figure 2. Schematic diagram of the rotation plane

The rotation surface is formed by rotating the MN curve 360 degrees around the central axis I-I. The area of the rotation surface is as follows [10]:

$$s(w) = 2\pi(w + x \tan \theta_m)(\pi/2 - \theta_m)(D/2 + w) \quad (8)$$

The velocity of the rotation surface is as follows:

$$v(w) = \frac{Q_m}{s(w)} \quad (9)$$

Based on Bernoulli equation and flow continuity equation, the following equation can be written:

$$p(w) + \frac{\rho}{2} v(w)^2 = p_a + \frac{\rho}{2} v_a^2 \quad (10)$$

$$v(w)s(w) = v_a s_a \quad (11)$$

The pressure at the seat's bottom is as follows:

$$p(w) = c_d^2 A_m^2 \left[\frac{2}{\rho} p_a + \frac{1}{s_a^2} - \frac{1}{s(w)^2} \right] (p_s - p_a) \quad (12)$$

Figure 3 shows the pressure distribution of the seat's bottom with different displacements.

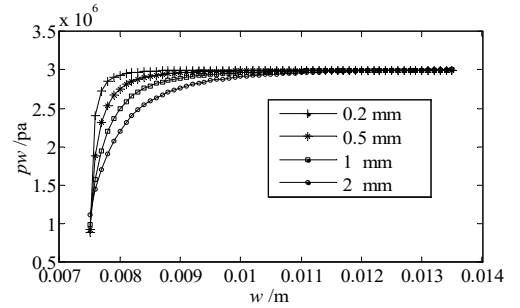


Figure 3. Pressure distribution of the seat's bottom

As it can be seen from the Figure 3, with the minimum displacement (0.2mm), the throttling effect is obvious and the pressure distribution varies sharply. For larger displacement, the pressure distribution varies smoothly.

III. FLOW SIMULATION UNDER FIXED OPENING

A. $k-\varepsilon$ model

The turbulence often occurs in the flow field of the HSV which can be described by Navier-Stokes equations. Several turbulence models provided by ANSYS Fluent can be used to simplify and solve the problem. In order to balance the accuracy and the compatibility with the two-phase cavitation model, the renormalization group (RNG) $k-\varepsilon$ model is chosen to solve the calculation.

Ignoring the viscosity and assuming that the fluid is incompressible[11], the turbulence kinetic energy k and dissipation rate ε are as follows [12]

$$\frac{\partial}{\partial t}(\rho k) + \frac{\partial}{\partial x_i}(\rho k u_i) = \frac{\partial}{\partial x_j}(\partial_k u_{eff} \frac{\partial k}{\partial x_j}) + G_k + G_b - \rho \varepsilon - Y_m - S_k \quad (13)$$

$$\begin{aligned} \frac{\partial}{\partial t}(\rho \varepsilon) + \frac{\partial}{\partial x_i}(\rho \varepsilon u_i) &= \frac{\partial}{\partial x_j}(\partial_\varepsilon u_{eff} \frac{\partial \varepsilon}{\partial x_j}) \\ &+ C_{1\varepsilon} \frac{\varepsilon}{k} (G_k + G_{3\varepsilon} G_b) - C_{1\varepsilon} \rho \frac{\varepsilon^2}{k} - R_\varepsilon + S_\varepsilon \end{aligned} \quad (14)$$

Where ρ and μ_{eff} denote the fluid density and the effective viscosity of fluid, respectively; G_k denotes the generation of turbulence kinetic energy due to mean velocity gradients; G_b denotes the generation of turbulence kinetic energy due to buoyancy, and Y_m denotes the contribution of the fluctuating dilatation incompressible turbulence to the overall dissipation rate; The variables α_k and α_ϵ indicate the inverse effective Prandtl numbers for k and ϵ , respectively; $C_{1\epsilon}$, $C_{2\epsilon}$, and $C_{3\epsilon}$ denote a constant related to the fluid model.

B. Geometry and meshing

A three-dimensional model is established by Pro/E, and the flow field model is extracted (displacement is 0.2mm). In order to reduce the computation time, half of the flow field is selected based on the symmetry plane.

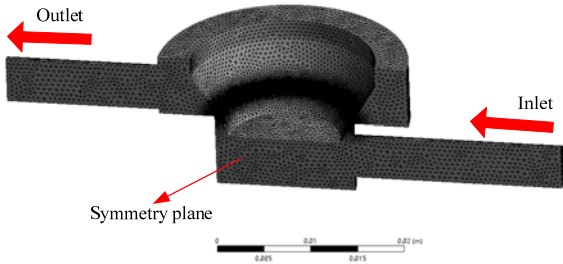


Figure 4. 3D mesh model

As it can be seen from Figure 4, the irregular mesh elements (tetrahedrons) are used to mesh the whole model and the element size is 0.5mm. However, in order to obtain the more accurate near-wall calculation, the mesh elements between the valve wall and the seat are intensified by a sphere of influence, in which the element size is 0.06mm. The average mesh quality reaches 0.84 which is checked by the mesh quality inspection tool.

C. Simulation under a fixed opening

As shown in Figure 5, the pressure distribution is concentrated at the valve orifice significantly. The pressure difference between the inlet and the outlet is close to 7MPa and the corresponding flow rate is shown in Figure 6.

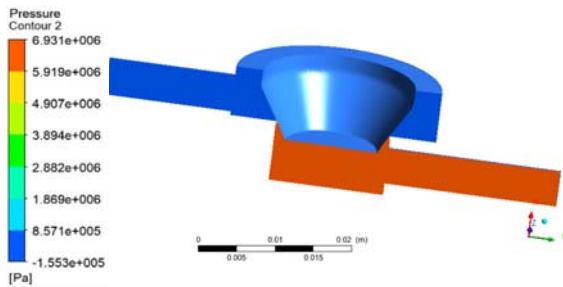


Figure 5. Simulation of pressure distribution

As it can be seen from Figure 6, the simulation results of flow rate agree with the theoretical results under different pressure differences, which demonstrate that the flow rate (@ $\Delta p=1\text{MPa}$) reaches 10L/min under a fixed opening (0.2mm). The maximum flow rate can be regulated by the adjustable displacement. Moreover, the simulation results of the steady flow force also agree with the theoretical results under different pressure differences, which is shown in Figure 7.

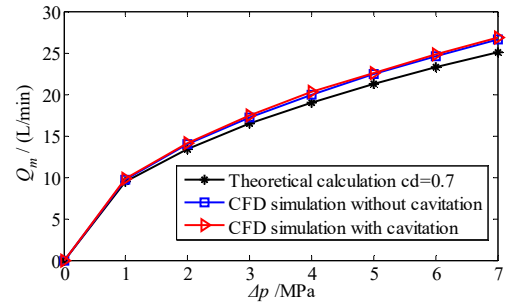


Figure 6. Flow rate comparison

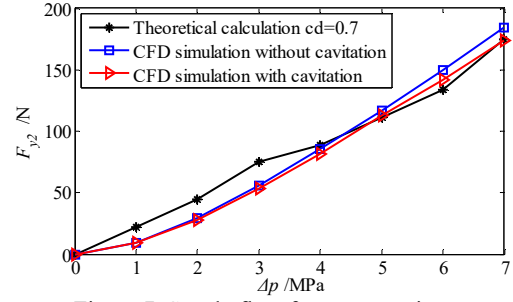
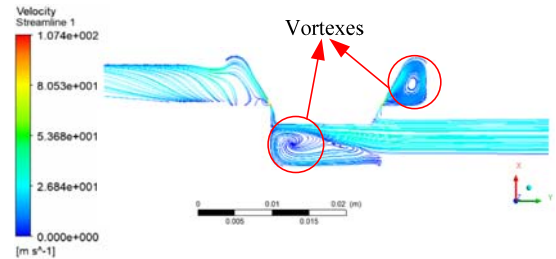
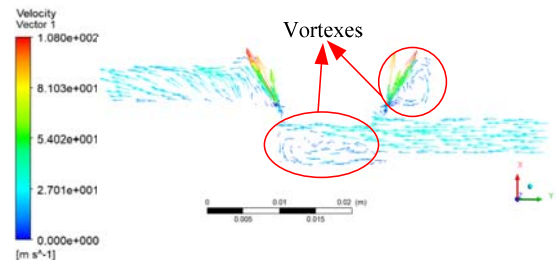


Figure 7. Steady flow force comparison

The velocity streamlines and velocity vectors are as shown in Figure 8 under the condition of steady flow. Two vortices are formed in the flow channel of the main valve and flow separation occurs as well. One is located at the bottom of the main valve and the other is located on the side of the main valve. This is due the viscosity of the corner's flow and the spin of the corner's flow actuated by main flow. The intensity of the latter is stronger than the former because the density of the latter streamline is bigger.



(a) Velocity streamlines



(b) Velocity vectors

Figure 8. Simulation of velocity under a fixed opening

Therefore, the energy in the main flow is extracted by the two vortices which reduce the energy efficiency. In addition, the vortices intensify the problem of fluid noise which can be solved by structure optimization. The volume fraction contour is shown in Figure 9. The volume fraction represents the intensity of cavitation effects which is observed obviously at the corner close to the outlet.

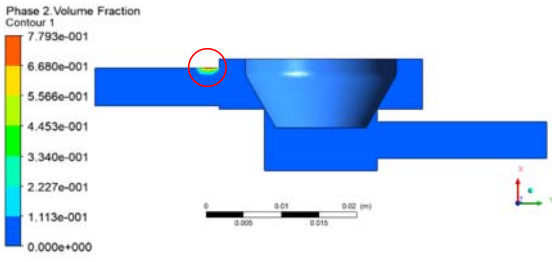


Figure 9. Simulation of volume fraction contour

IV. TRANSIENT FLOW SIMULATION

A. Mesh Model and Boundary Conditions

In order to study the influences of high frequency switching on the transient pressure and the transient velocity, in this paper, the dynamic mesh technique is used to simulate the movement of the main valve (switching frequency is 20 Hz and duty cycle is 50%). The displacement of the main valve is pre-designed, which can be observed in Figure 10. A two-dimensional fluid model is selected to reduce the computational cost (Figure 11). The wall of the main valve is defined as a rigid wall and other parts are defined as stationary walls. The velocity of the main valve is defined by the USER PROFILE. Constant pressure (7MPa) is imposed for the inlet boundary condition and constant pressure (0.1MPa) is defined as the outlet boundary condition. In a finite differencing scheme of the governing equations, the finite control volume method is employed and the second-order upwind difference scheme is applied.

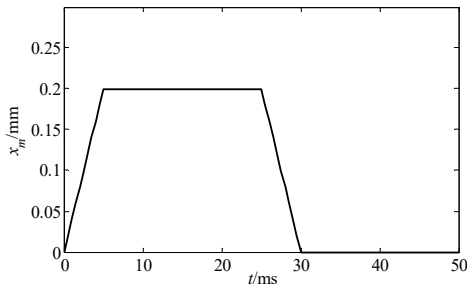


Figure 10. The movement of the main valve

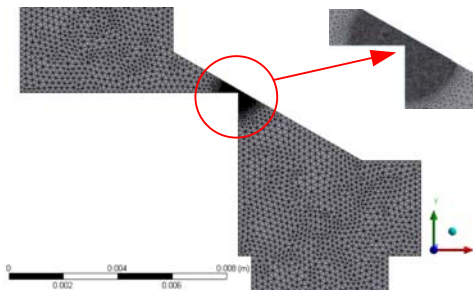
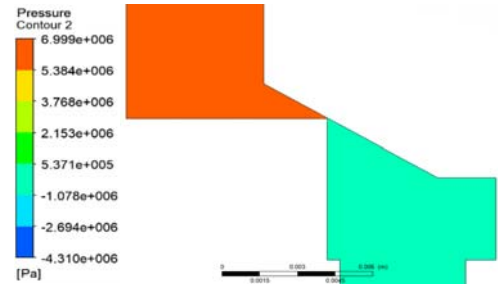


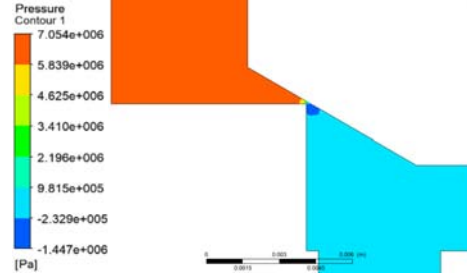
Figure 11. 2D mesh model

B. Pressure Distribution

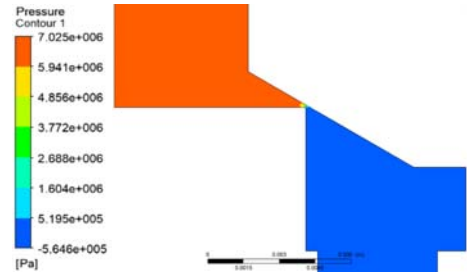
Figure 12 shows the pressure distribution contours under different transient times. The pressure is rapidly diminished at the valve orifice due to the throttling. On this occasion, cavitation is easy to happen which has a big influence on hydraulic components, such as flow rate fluctuation, vibration and noise.



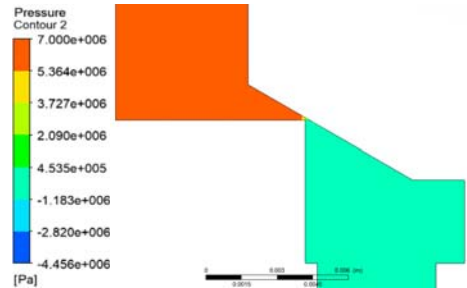
(a) 0 ms (Almost closing stage)



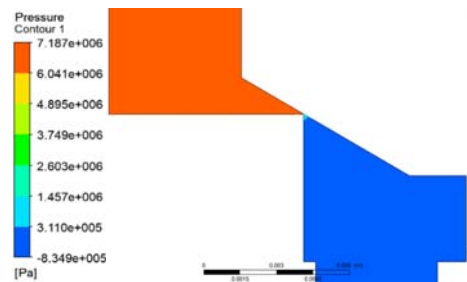
(b) 2.5 ms (Half open stage)



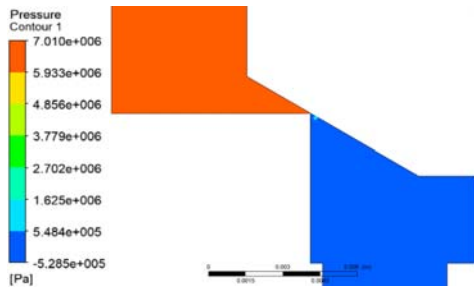
(c) 5 ms (Fully open stage)



(d) 25 ms (Fully open stage)



(e) 27.5 ms (Half closing stage)



(f) 50 ms (Almost closing stage)

Figure 12. Pressure distribution contours under different transient times

The inlet pressure slightly fluctuates in the opening stage (Figure 12b). But when the valve reaches the fully open, the inlet pressure returns back to initial pressure (Figure 12d). Conversely, the inlet pressure significantly fluctuates in the closing stage (Figure 12e). When the valve reaches the almost closing stage, the inlet pressure also returns back to initial pressure (Figure 12f). In addition, the transient pressure distribution is different with the pressure distribution under the fixed opening.

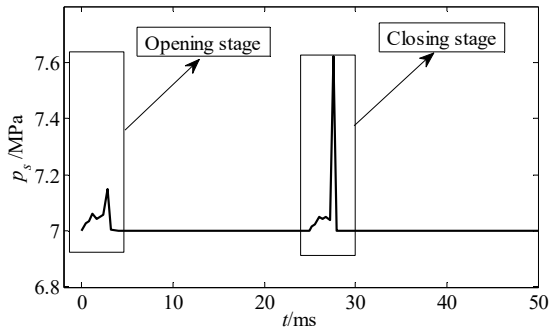
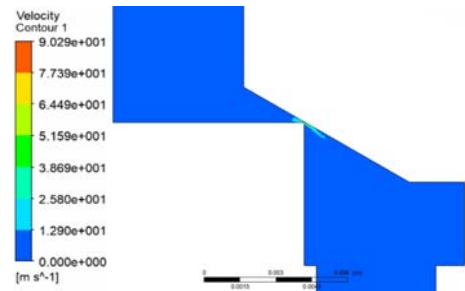


Figure 13. Changing of the inlet pressure in a period

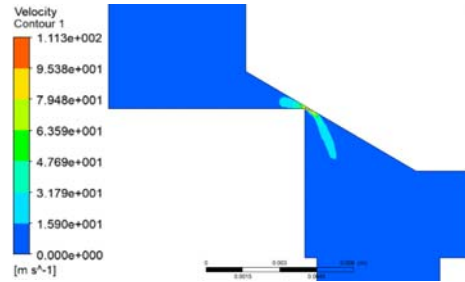
The same results can be observed in Figure 13. The sudden rise of inlet pressure occurs in the opening stage and closing stage, and the latter is more severe (8.6%), which is related to the fluid hammer. This is because that the rate of change in the momentum of a system is equal to sum of the forces exerted on the system.

C. Velocity Distribution

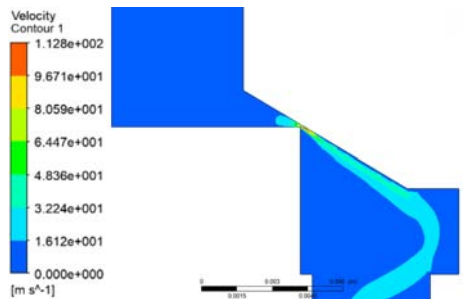
Figure 14 shows the velocity distribution contours under different transient times. The velocity of the fluid varies sharply at the valve orifice due to the throttling. The velocity of fluid reaches 123.5m/s in the fully open stage which can be seen from Figure 14 (d), but then drops to 95.1m/s in the half closing stage which is probably caused by the changing flow coefficient. The jet characteristic at valve orifice is complicated in different stages, and the eddy occurs at the corner closed to the outlet which can result in loss of energy. In addition, although the fluid dynamic noise is not caused directly by the fluid velocity gradient at the valve orifice, there is a certain relationship between the two issues which should be paid attention to.



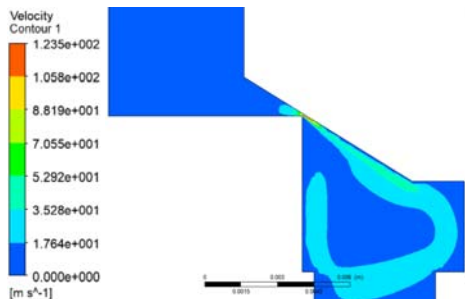
(a) 0 ms (Almost closing stage)



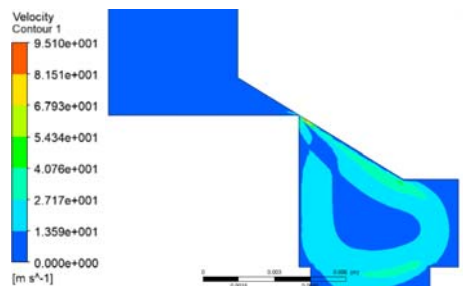
(b) 2.5 ms (Half open stage)



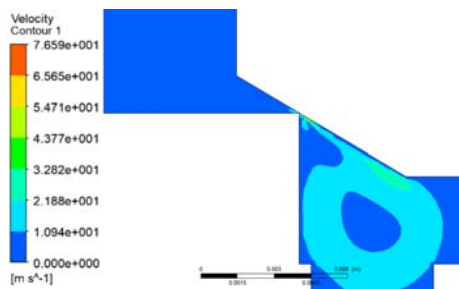
(c) 5 ms (Fully open stage)



(d) 25 ms (Fully open stage)



(e) 27.5 ms (Half closing stage)



(f) 50 ms (Almost closing stage)

Figure 14. Velocity distribution contours under different transient times

V. CONCLUSION

In this study, CFD simulations are carried out to achieve a good understanding of the flow field of the main poppet valve in LFHSV.

The flow simulation under fixed opening demonstrates that, the simulations results of flow rate and the steady flow force agree with the theoretical calculation results; it was also found that two vortexes are formed in the flow channel of the main valve due to the viscosity of the corner's flow and the spin of the corner's flow actuated by the main flow; and that the vortexes would extract the energy from the main flow and intensify the fluid noise.

Using the pressure and the velocity distribution, the cavitation was studied and explained based on the transient flow simulation results. In addition, the pressure peak at the inlet can be observed and quantified (8.6%). The pressure peak is related to the fluid hammer and the fluid dynamic noise, especially in the closing stage.

The simulation results serve as guidance for the optimal structural designs of the large flow rate High speed on/off valves.

REFERENCES

- [1] Pan M, Plummer A. Digital switched hydraulics. *Frontiers of Mechanical Engineering*, 2018, 13(2):225-231.
- [2] Linjama M, Laamanen A, Vilenius M. Is it time for digital hydraulics. *The Eighth Scandinavian International Conference on Fluid Power*. 2003.
- [3] Jiao ZX, Liu XC, Shang YX, et al. An integrated self-energized brake system for aircrafts based on a switching valve control. *Aerospace Science & Technology*, 2017, 60:20-30.
- [4] Meng AH, Song J. Linear control performance improvement of high speed on-off valve controlled by PWM. *SAE International Journal of Commercial Vehicles*, 2015, 8(2015-01-2672): 283-292.
- [5] Linjama M. Digital fluid power: State of the art. *12th Scandinavian International Conference on Fluid Power*, Tampere, Finland, May. 2011: 18-20.
- [6] Wu S, Zhao XY, Li CF, et al. Multi-objective optimization of a hollow plunger type solenoid for high speed on/off valve. *IEEE Transactions on Industrial Electronics*, 2018, 65(4): 3115-3124.
- [7] Xiao-xia G, Jia-hai H, Long Q, et al. Transient flow field characteristic analysis of poppet valve based on dynamic mesh 6DOF technique. *Fluid Power and Mechatronics (FPM), 2015 International Conference on. IEEE*, 2015: 928-933.
- [8] Gang Y, Fabing T, Baoren L, et al. Optimization of internal flow channel of a right-angle globe valve based on CFD. *Fluid Power and Mechatronics (FPM), 2015 International Conference on. IEEE*, 2015: 144-147.
- [9] Dianrong G, Yiqun W, Gongxin S. Numerical simulation and experimental visualization of the flow field inside hydraulic control poppet valve. *Chinese Journal of Mechanical Engineering*, 2002, 38(4): 66-70.
- [10] Zheng S J, Quan L, Wang W Q. Steady Flow Force of Truncated Poppet Valve with Convergent Flow. *Chinese Hydraulics & Pneumatics*, 2014(8):55-60.
- [11] Jalil J M, Ahmed S T, Xue Y, et al. Experimental and numerical investigation of fluid flow of truncated conical poppet valve[J]. *International journal of fluid power*, 2015, 16(1): 25-34.
- [12] Zhang J, Wang D, Xu B, et al. Experimental and numerical investigation of flow forces in a seat valve using a damping sleeve with orifices. *Journal of Zhejiang University-SCIENCE A*, 2018, 19(6): 417-430.